Proposal for the search for exotic spin-spin interactions at the micrometer scale using functionalized cantilever force sensors

Qian Wang,[1] Ze Ouyang,[2] Yu Lu,[1] Jianbo Wang,[3] Lin Zhu,[1] and Pengshun Luo[1,*]

[1]*MOE Key Laboratory of Fundamental Quantities Measurement, Hubei Key Laboratory of Gravitation and Quantum Physics, School of Physics, Huazhong University of Science and Technology, Wuhan 430074, China*

[2]*School of Physics, Huazhong University of Science and Technology, Wuhan 430074, China*

[3]*Huazhong Institute of Electron-Optics, Wuhan National Laboratory for Optoelectronics, Wuhan 430223, China*

(Received 13 July 2022; accepted 14 December 2022; published 5 January 2023)

Spin-dependent exotic interactions can be generated by exchanging hypothetical bosons, which were introduced to solve some puzzles in physics. Many precision experiments have been performed to search for such interactions, but no confirmed observations have been made. We propose new experiments to search for the exotic spin-spin interactions that can be mediated by axions or Z′ bosons. A sensitive functionalized cantilever is utilized as a force sensor to measure the interactions between the spin-polarized electrons in a periodic magnetic source structure and a closed-loop magnetic structure integrated on the cantilever. The source is set to oscillate during data acquisition to modulate the exotic force signal to high harmonics of the oscillating frequency. This helps to suppress the spurious signals at the signal frequency. Different magnetic source structures are designed for different interaction detections. A magnetic stripe structure is designed for Z′-mediated interactions, which are insensitive to the detection of axion-mediated interactions. This allows us to measure the coupling constant of both if we assume that both exist. With the force sensitivity achievable at low temperatures, the proposed experiments are expected to search for parameter spaces with much smaller coupling constants than the current stringent constraints from micrometer to millimeter range. Specifically, the lower bound of the parameter space will be 7 orders of magnitude lower than the stringent constraints for Z′-mediated interactions, and an order of magnitude lower for axion-mediated interactions, at the interaction range of 10 μm.

DOI: 10.1103/PhysRevD.107.015005

I. INTRODUCTION

The search for spin-dependent exotic interactions has recently attracted attention in particle physics related fields [1–3]. These interactions can occur between two fermions when new spin-0 or spin-1 bosons are exchanged [4–9], which has been proposed to address some mysteries in physics, such as the strong *CP* problem [10–13], dark matter [14,15], dark energy [16–18], and the hierarchy problem [19,20]. Among them, the axion was one of the prominent bosons introduced to solve the strong *CP* problem and is now a promising candidate for dark matter [21–23]. As Moody and Wilczek first pointed out, spin-dependent exotic interactions can arise through axion exchange [4]. In a more general discussion by Dobrescu and Mocioiu, the spin-dependent potentials were classified into 15 types according to their mathematical spin-momentum structures [8]. These potentials have recently been rederived in a form that clearly shows the relationship between the potentials and the bosons mediating them [9] and shows that the interactions can be generated by pseudoscalar coupling, vector coupling, and axial-vector coupling between fermions and generic spin-0 or spin-1 bosons.

In this paper, we propose new experiments to explore the following spin-spin interactions between electrons, enumerated as V_2 and V_3 in Ref. [8]:

$$V_2 = \frac{g_A^e g_A^e}{4\pi\hbar c}\frac{\hbar c}{r}(\hat{\sigma}_1 \cdot \hat{\sigma}_2)e^{-r/\lambda}, \tag{1}$$

$$V_3 = -\frac{g_p^e g_p^e}{4\pi\hbar c}\frac{\hbar^3}{4m_e^2 c}\left[(\hat{\sigma}_1 \cdot \hat{\sigma}_2)\left(\frac{1}{\lambda r^2}+\frac{1}{r^3}\right) - (\hat{\sigma}_1 \cdot \hat{r})(\hat{\sigma}_2 \cdot \hat{r})\left(\frac{1}{\lambda^2 r}+\frac{3}{\lambda r^2}+\frac{3}{r^3}\right)\right]e^{-r/\lambda}, \tag{2}$$

where $g_A^e g_A^e/4\pi\hbar c$ and $g_p^e g_p^e/4\pi\hbar c$ are the dimensionless coupling constants, $\hbar$ is the Dirac constant, c is the speed of

[*]pluo2009@hust.edu.cn

light in vacuum, $\hat{\sigma}_1$ and $\hat{\sigma}_2$ are the unit spin vectors of the electrons, r is the distance between them, $\hat{r}$ is the unit relative position vector, and λ is the interaction range. Here $\lambda = \hbar/m_b c$ is the reduced Compton wavelength of the hypothetical boson that mediates the interaction and m_b is its mass. The V_2 potential can be mediated by a spin-1 Z′ boson via axial-vector coupling [5,6,8,9]. The V_3 potential can be mediated by spin-0 pseudoscalar bosons such as axions and axionlike particles [4,8,9].

Various techniques have been applied or proposed to search for these exotic potentials, including atomic and optical precision measurements [24–36], mechanical sensors [28,37–40], and superconducting quantum interference devices [41]. Thus far, there has been no convincing evidence for the existence of new interactions, but experiments have placed increasingly stringent constraints on them. For the V_2 interaction in the interaction range extending from 0.1 μm to 1 mm, the most stringent constraints are set by the experiments with trapping strontium ions [29] and quantum diamond sensors [34]. An analysis of helium atomic spectra has been used to impose the strictest constraints on V_3 interactions [32]. The above constraints have been obtained by comparing the experimental data with a theoretical calculation of a magnetic dipole-dipole interaction. The results depend on the experimental measurement noise, the accuracy of the theoretical calculation, and how well the experimental data match the theoretical values.

Here we propose searching for exotic interactions by measuring the force between two magnetized objects with a cantilever. To avoid the high precision requirement for calculating electromagnetic effects, we employ periodic magnetic structures that can generate spatially varied exotic force signals so that we can distinguish between the signals of interest from interfering forces. For another interacting object, a closed magnetic loop enclosed with superconducting thin film shielding is used to suppress the magnetic force. Different periodic magnetic structures are designed for different interaction detections, which enables us to perform joint data analysis under the assumption that both V_2 and V_3 could exist, whereas each was usually considered independently in the previous literature. Finally, using a sensitive cantilever allows us to probe the exotic interactions at distances in the range of micrometers with high precision.

This paper is organized as follows. Section II illustrates the experimental scheme. Section III describes the experimental designs, including the probe and source structures in detail, as well as the expected force signal and parameter space that can be explored. In Sec. IV, we discuss the influence of the spurious forces likely to appear in the experiments. The conclusions are given in Sec. V.

II. EXPERIMENTAL SCHEME

The experiments are schematically shown in Fig. 1. A cantilever is used as a force sensor to measure the exotic interaction between the spin-polarized electrons in the closed-loop magnetic structure (CLMS) on the cantilever and that in another source, with the two separated by several micrometers. The source is a periodic magnetic structure which is expected to produce a spatially periodic exotic potential field. Thus, once the source is driven to oscillate by a piezoelectric element, a time-varying force is expected to exert on the cantilever and make it oscillate. The displacement of the cantilever can be measured by a fiber interferometer. In the frequency domain, the mechanical response of a force acting on the cantilever is

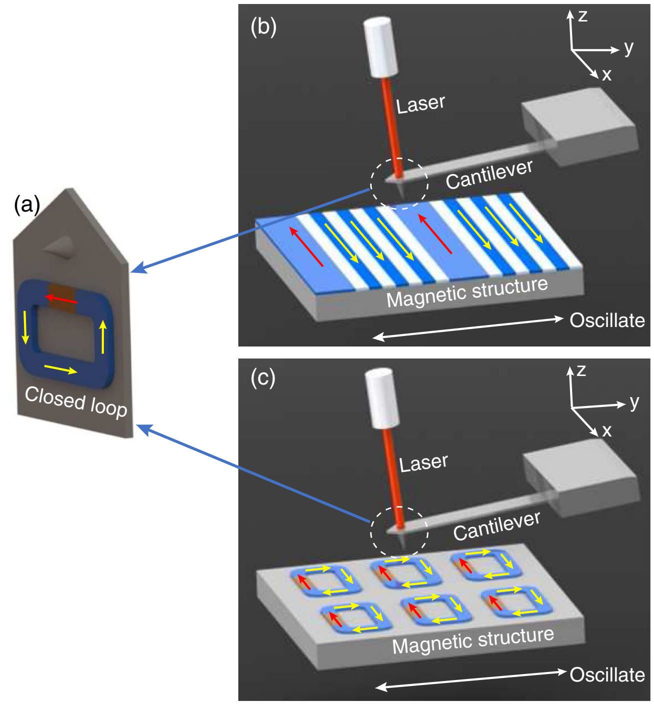

FIG. 1. Schematic of the proposed experiments. (a) End part of the cantilever with the CLMS integrated. The arrows indicate the direction of magnetization, with the yellow arrows representing the magnetization of the soft magnet and the red arrow representing the magnetization of the permanent magnet. (b) Proposed experimental searches for V_2 interactions. A fiber interferometer is used to measure the displacement of the cantilever. The spin-polarized source is designed as alternative antiparallel spin-polarized magnetic stripes. (c) Proposed experimental searches for V_3 interactions. The spin-polarized source is designed as a periodic array of the closed-loop magnetic structures.

$$z(\omega) = \frac{1}{m} \frac{F_z(\omega)}{\omega_0^2 - \omega^2 + \frac{i\omega\omega_0}{Q}}, \tag{3}$$

where the subscript z indicates the force along the z axis, $z(\omega)$ denotes the displacement of the cantilever in the frequency domain, ω_0 is the intrinsic resonant angular frequency of the cantilever, Q is the quality factor of the cantilever, and m denotes the total effective mass of the cantilever.

The exotic force F_z is calculated as

$$F_z = -\frac{\partial}{\partial d}\int n_s n_p V(r)\mathrm{d}V_s\mathrm{d}V_p, \tag{4}$$

where n_s is the number density of the spin-polarized electrons in the periodic source structure and n_p is that in the CLMS. The integral is performed on the exotic potential $V(r)$ over volumes of both the source (V_s) and the CLMS (V_p). The force is obtained by taking the derivative of the integral with respect to d, the distance between the CLMS and the spin-polarized source.

The sources are specially designed for different exotic interactions. We use magnetic stripes with periodic antiparallel spin polarization to detect the exotic potential V_2 [see Fig. 1(b)]. This structure can generate a periodic V_2 signal, while creating a negligible V_3 force if we make the stripes sufficiently long. The magnetic field generated by the magnetic stripes lies in the plane and closes at the end of the stripes, so the magnetic field produced at the CLMS is small and the induced magnetic force is negligible. However, the V_2 potential decays exponentially with distance so that only the segments of the stripes near the CLMS contribute to the force. Another structure, made of the CLMS array, is used for the detection of V_3 [see Fig. 1(c)]. It should be noted that this structure also generates a V_2 signal, so we can combine the two experiments to measure the strength of both interactions while assuming the presence of both. To reduce the disturbance of the Casimir force and electrostatic force, the surfaces of the sources are coated with a layer of metallic thin film or superconducting thin film.

III. EXPERIMENTAL DESIGN

A. Cantilever with a closed-loop magnetic structure

Searching for the spin-spin interactions requires the use of spin-polarized objects; thus, the magnetic force between the objects is a key factor to consider. To reduce the stray field produced by the object, we consider using a cantilever with a CLMS attached at its end. The CLMS is made of a soft magnetic loop (e.g., $Ni_{80}Fe_{20}$) with a permanent magnetic segment (e.g., $SmCo_5$) embedded in it, as shown in Figs. 1(a) and 2. The permanent magnet can magnetize the soft magnetic material, and the electron spins are then polarized along the loop, thereby providing the source of electron spins for the spin-spin interactions. As the magnetization is roughly closed in a loop, the CLMS creates a very small stray field outside of it.

The finite element analysis (FEA) is conducted to simulate the magnetization and stray field of the CLMS. Figure 2 shows the simulated distribution of the magnetic flux density at its remnant state. We can see that a toroidal magnetization forms, except for a relatively small leakage magnetic field around the junctions between the two different materials. The leakage magnetic field is on the order of milliteslas, which can create a magnetic force larger than the force sensitivity of the cantilever in the V_3 search experiment. Since the leakage magnetic field is smaller than the lower critical field of the NbTi superconductor, it can be shielded by enclosing the CLMS inside the NbTi thin films. According to the simulation, using 1.5-μm-thick NbTi thin film can shield the magnetic field down to 10^{-8} T, which will be discussed in detail in Sec. IV.

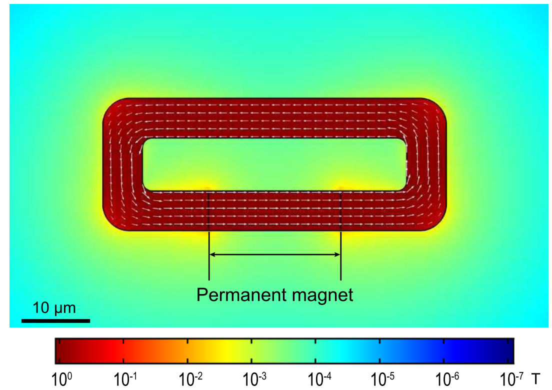

FIG. 2. FEA simulation of the magnetic properties of the CLMS. The arrows indicate the magnetization in the central plane of the CLMS, and the color scale shows the magnitude of the magnetic flux density. A magnetization of 800 kA/m is used for the permanent magnet, and the soft magnet is simulated with a relative magnetic permeability of 8000.

The magnetic loops can be microfabricated on a silicon on insulator (SOI) wafer with a NbTi thin film predeposited. After the magnetic loops are fabricated, another NbTi layer is deposited on the structure to enclose all the magnetic materials. By selectively etching off the handle layer of the SOI wafer, we can leave the CLMS on the suspended silicon device layer, which enables us to cut the structure with a focused ion beam and then transfer it to a customized cantilever with a tip height of ∼10 μm.

B. Minimum detectable force

The minimum detectable force depends on the thermal noise of the cantilever and the displacement measurement noise of the fiber interferometer. The thermal noise of the cantilever is given as

$$S_{F_T}^{1/2}(f) = \sqrt{\frac{2kk_BT}{\pi f Q}}, \tag{5}$$

where k is the spring constant of the cantilever, chosen to be 0.02 N/m, k_B is the Boltzmann constant, T is the temperature, and Q is the quality factor of the cantilever. The experiments need to be conducted at low temperatures for superconducting shielding to work. Using the base temperature (6 K) of our instrument, we calculate the thermal noise to be 2.0×10^{-15} N/$\sqrt{\mathrm{Hz}}$ by conservatively

TABLE I. Experimental parameters used in the proposed experiments.

Parameter	Value	Unit
CLMS		
Length of outer loop	52	μm
Width of outer loop	20	μm
Length of inner loop	40	μm
Width of inner loop	8	μm
Thickness	1	μm
Spin-polarized source in V_2 experiment		
Length of magnetic stripes	6	mm
Width of wide stripes	6	μm
Width of narrow stripes	2	μm
Gap between the stripes	2	μm
Thickness of stripes	1	μm
Spin-polarized source in V_3 experiment		
Distance between CLMSs (x direction)	8	μm
Distance between CLMSs (y direction)	8	μm
Probe		
Diagonal length of tip	6	μm
Tip height	10	μm
Cantilever length	450	μm
Cantilever width	48	μm
Cantilever thickness	1	μm
Spin-source distance	10	μm
Number density of polarized electrons	6.6×10^{28}	

assuming that $Q = 10000$. The displacement measurement noise of 100 fm/$\sqrt{\mathrm{Hz}}$ can be achieved at the frequency of interest. Given the acquisition time of 1000 s and signal frequency of 25.8 Hz [42], the minimum detectable force is estimated to be 8.9×10^{-17} N as the quadrature sum of the two contributions.

C. Search for the V_2 interaction

To search for the V_2 interaction, we use periodic magnetic stripes of different widths as another source [see Fig. 1(b)]. Since the coercive field of the narrow stripes is larger than that of the wide stripes due to shape dependent demagnetization, the magnetic structure can be prepared in an antiparallel state in the following way. First, let us apply a magnetic field large enough to magnetize all the stripes in the same direction, say, the $+x$ direction; then we reverse the field to simply flip the magnetization of the wide stripes. Since each stripe has a near square hysteresis loop, the antiparallel state remains after the magnetic field is removed. Such structures were successfully fabricated in a previous experiment [42], where their surfaces were further coated with gold films to reduce the contribution of the Casimir force and the electrostatic force.

The preliminary design parameters of the structure are listed in Table I. The expected V_2 force is numerically calculated as a function of the lateral position y for $\lambda = 10$ μm; the result is shown in Fig. 3(a). Here the

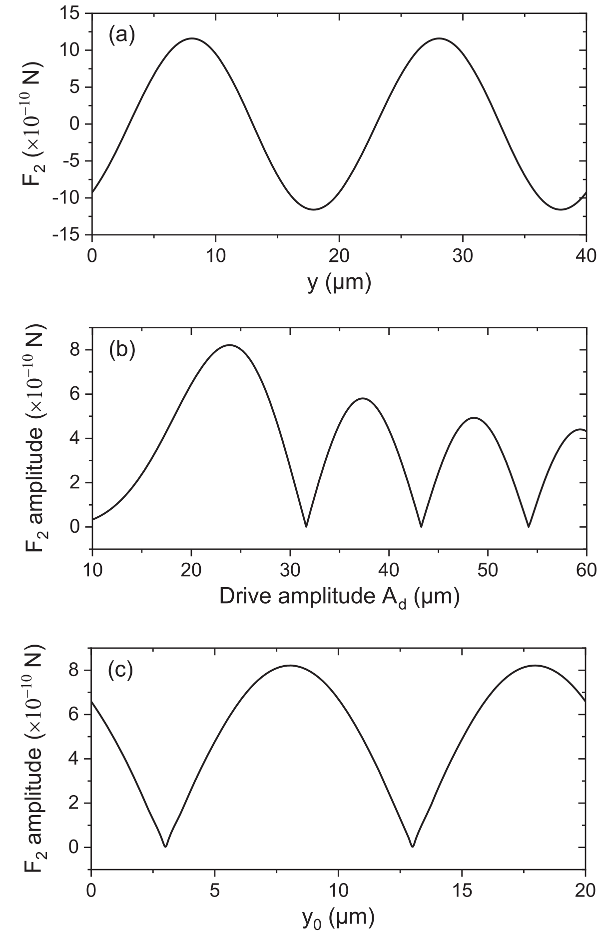

FIG. 3. (a) The expected V_2 force varies with the relative position along the y direction. (b) The V_2 force amplitude at $6f_d$ as a function of the driving amplitude. (c) The V_2 force amplitude at $6f_d$ as a function of y_0. In the calculation, $g_A^e g_A^e/4\pi\hbar c$ is set to 1.8×10^{-19} with $\lambda = 10$ μm.

coupling constant $g_A^e g_A^e/4\pi\hbar c$ is chosen to be 1.8×10^{-19}, which is the most stringent constraint given by the experiment based on quantum diamond sensors to date. The number density of spin-polarized electrons n in the structure is given by

$$n = \frac{M r_{sa}}{\mu_B}, \tag{6}$$

where M is the magnetization of the CLMS, μ_B is the Bohr magneton, and r_{sa} is the ratio of the spin to all magnetic moments, depending on the material composition [43]. The V_2 force is periodic with y and varies with an amplitude of 8.2×10^{-10} N, which is about 7 orders of magnitude larger than the minimum detectable force of the cantilever. During data acquisition, we drive the source to oscillate as $y = y_0 + A_d \cos(2\pi f_d t)$ and record the resulting time-varying signal. The exotic force signal is then modulated to the harmonic frequencies, which helps us to separate the spurious signals from the signal of interest. The exotic force amplitude at the mth harmonic frequency is given by

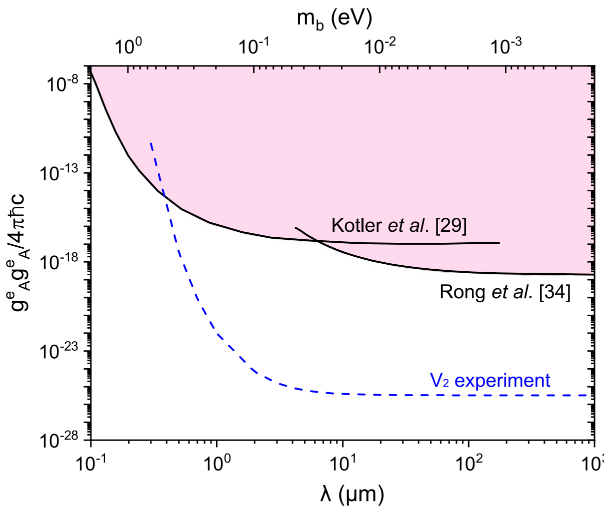

FIG. 4. Constraints on the coupling constant of the V_2 potential. The dashed line represents the lower bound of the parameter space that the proposed experiment can explore.

$$F_m(y_0) = \sum_{n=-\infty}^{+\infty} i^m J_m(k_n A_d)[f(k_n)e^{ik_n y_0}], \quad (7)$$

where $f(k_n)$ is the nth coefficient of the Fourier series expansion of $F_z(y)$, $k_n = n2\pi/\Lambda$, with Λ being the magnetic structure period, and J_m is a Bessel function of order m. Figure 3(b) shows the V_2 force amplitude at $6f_d$ as a function of the driving amplitude A_d. We can see that the optimal value for A_d is 23.9 μm, which maximizes the force amplitude at $6f_d$.

The force amplitude is a periodic function of y_0, the equilibrium position of the oscillation. Therefore, we can collect data by changing y_0 over a range larger than one period. The expected result is shown in Fig. 3(c). If we do not observe any periodic signal in such a measurement, the V_2 force must be lower than the minimum detectable force. Based on the preliminary design parameters, the potential limit on the coupling constant $g_A^e g_A^e/4\pi\hbar c$ can be obtained, which is shown in Fig. 4. The result indicates that we can explore a range of coupling constants down to 7 orders of magnitude lower than the current strictest constraint at $\lambda = 10$ μm.

D. Search for the V_3 interaction

The magnetic stripe structure is not a suitable source for the search for the V_3 interaction. The V_3 force between the CLMS and the stripe structure is greatly suppressed because of the subtracting terms in Eq. (2) canceling each other for sufficient long magnetic stripes. This makes the magnetic stripe structure sensitive only to V_2 detection. To search for the V_3 interaction, we need to cut the stripes into segments with optimal length and spacing. To keep the magnetic force low, we choose to use the CLMS array as the source of the V_3 detection, as shown in Fig. 1(c). Each CLMS in the array has the same dimensions as the CLMS on the cantilever. The spacing between them is optimized, and the values are listed in Table I. To further reduce the magnetic force below the minimum detectable force, the CLMS array needs to be shielded by superconducting films, which will be discussed in Sec. IVA.

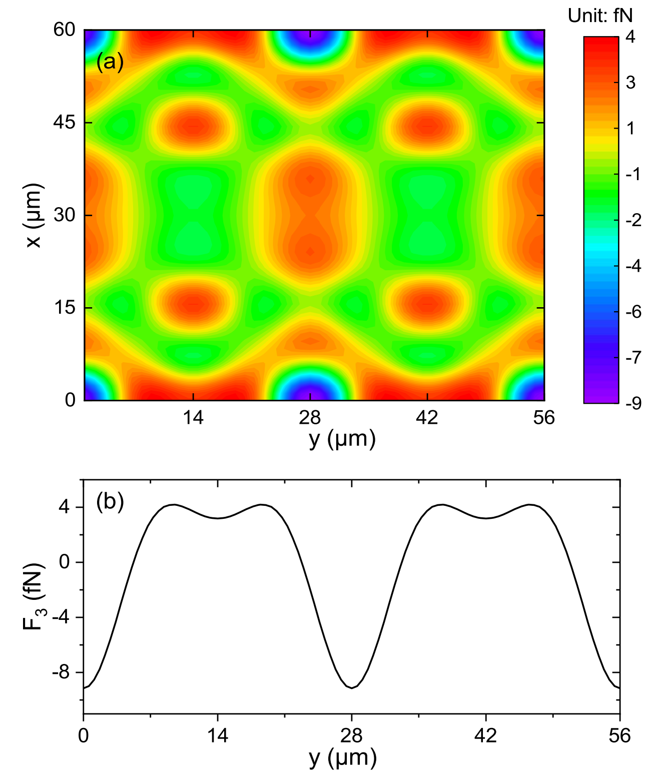

FIG. 5. (a) The expected V_3 force map in the x-y plane at a constant probe-source distance. (b) The V_3 force varies along the y axis at $x = 0$. In the calculation, $g_p^e g_p^e/4\pi\hbar c$ is set at 1.0×10^{-8} with $\lambda = 10$ μm.

The V_3 force, which depends on both x and y, can be calculated numerically. Figure 5(a) shows an expected force map for $g_p^e g_p^e/4\pi\hbar c = 1.0 \times 10^{-8}$ and $\lambda = 10$ μm. As expected, the force is periodic in both the x and y directions. As in the V_2 search, we plan to modulate the V_3 force to the harmonics of the driving frequency by oscillating the source in the y direction. By acquiring data at different points on a plane with a constant probe-source distance, we will obtain a map of force amplitude at the harmonic frequency. The maximum likelihood method can be used to determine the coupling constant for every λ by comparing the experimental data with the expected theoretical values, as we did previously [42,44,45]. Assuming that the experimental results are limited by the minimum detectable force, we can obtain the lower bound of the coupling constant that can be explored in this experiment. As shown in Fig. 6, more than an order of magnitude improvement in V_3 detection can be achieved at $\lambda = 10$ μm.

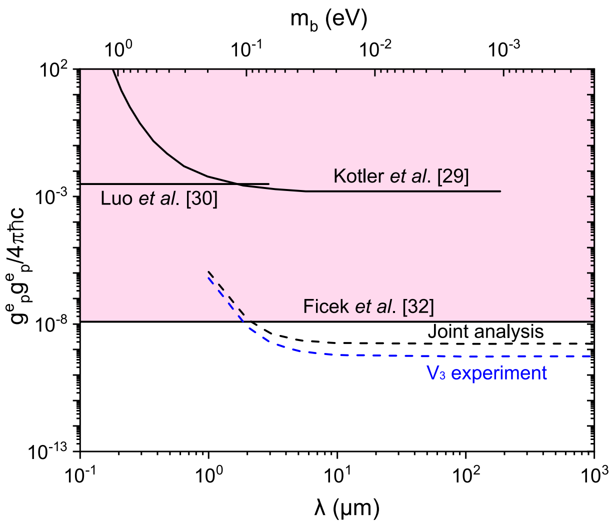

FIG. 6. Constraints on the coupling constant of the V_3 potential. The blue dashed line represents the lower bound of the parameter space that the proposed experiment can probe, assuming that only V_3 exists. The black dashed line represents the lower bound, assuming that both V_2 and V_3 could exist.

If we consider more generally that both the V_2 and V_3 interactions may exist, we can first determine the coupling constant for the V_2 interaction as the stripe source structure is insensitive for the V_3 detection. With the V_2 coupling constant, we can subtract the V_2 interaction in the V_3 experiment to get the coupling constant of the V_3 interaction. If no signal of new interaction is observed in either experiment, a joint data analysis would yield a limit on the V_3 coupling constant, which is approximately 3 times higher than that in which only one interaction is considered.

IV. SPURIOUS FORCES

To perform experiments with precision limited by the minimum detectable force of the cantilever, we need to suppress spurious forces to a negligible level. The dominant spurious forces in the experiments are the magnetic force, the Casimir force, and electrostatic forces. We will now discuss them one by one.

A. Magnetic force

For the search for spin-spin interactions, the magnetic force between the two objects is the main spurious effect to be considered. In the search for the V_2 interaction, we evaluate the magnetic force by numerically integrating the magnetic dipole-dipole interaction between two spins, which are given by

$$V_m = -\frac{\mu_0 \gamma_e^2 \hbar^2}{16\pi r^3}[3(\hat{\sigma}_1 \cdot \hat{r})(\hat{\sigma}_2 \cdot \hat{r}) - (\hat{\sigma}_1 \cdot \hat{\sigma}_2)], \quad (8)$$

where μ_0 is the vacuum permeability and γ_e is the gyromagnetic ratio of the electron. The magnetic force

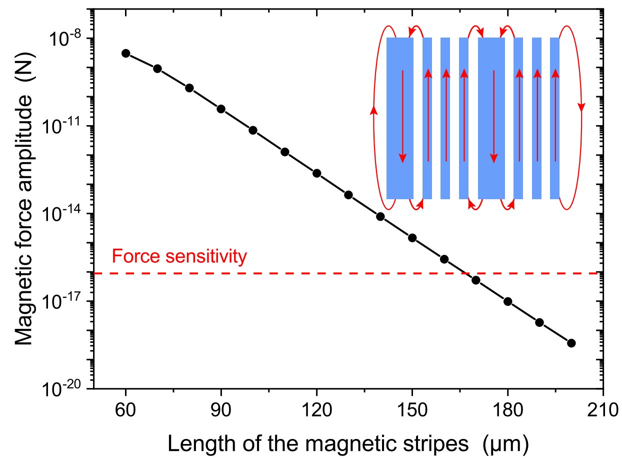

FIG. 7. The dependence of the magnetic force amplitude on the length of the magnetic stripes. The minimum detectable force is presented as a dashed line. Inset: schematic drawing of the magnetic field lines generated by the stripes.

varies periodically with the stripe structure, but its peak-to-peak value decreases rapidly with the length of the stripes, as shown in Fig. 7. The reason is that the magnetic field generated by the stripes is mainly in plane and closed at the end of the stripes (see the inset of Fig. 7); thus, the magnetic field is negligibly small at the probe's location that is in the center and near the surface of the source structure. The magnetic force is shown to be smaller than the minimum detectable force when the length of the stripe is longer than 170 μm. Since the real length of the magnetic stripes will be 6 mm, the magnetic force is expected to be much below the minimum detectable force.

The imperfections in the fabrication of the stripes may generate an unexpected magnetic field around the superconducting film-coated CLMS, thus inducing a magnetic force. In order to get a simple idea of how large the force can be, we simulate the imperfections with an array of magnetic cubes. The gaps between the cubes are set to the period of the magnetic stripes in the y direction and the length of the CLMS in the x direction; thus, one imperfection exists in the area of a CLMS. Their magnetization is set to 800 kA/m along the z direction to generate the maximum magnetic force. We evaluate the force between the magnetic cubes and the superconducting shielded CLMS with the FEA and find that the volume of the cube should not exceed $\sim 150 \times 150 \times 150\ \mathrm{nm}^3$ to make the force amplitude lower than the minimum detectable force, as shown in Fig. 8.

In the search for the V_3 interaction, the magnetic force is evaluated with the FEA. We first calculate the lateral position dependence of the magnetic force between two CLMSs at a distance of $d = 10$ μm. The result is shown in Fig. 9(a). Owing to the closed-loop design, the peak magnetic force is reduced to $\sim 10^{-11}$ N but is still much larger than the minimum detectable force. To further

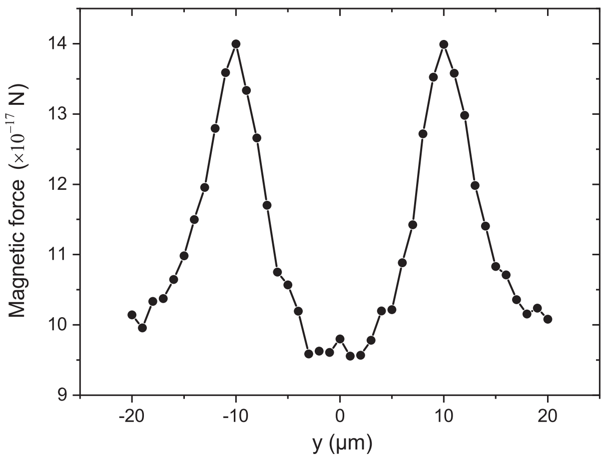

FIG. 8. Calculated magnetic force between the magnetized cubes and the superconducting shielded CLMS with the FEA. The volume of the cube is $150 \times 150 \times 150$ nm^3.

suppress the magnetic force, we propose encapsulating the CLMSs with superconducting thin films. The closed-loop design reduces the stray field down to the critical field of the superconductor and then makes superconducting magnetic shielding possible. The magnetic shielding effect is simulated with the FEA (see the details in the Appendix). According to the simulation, a 1.5-μm-thick superconducting film can effectively shield the magnetic field down to 2.4×10^{-11} T [see Fig. 9(b)]. The magnetic force acting on the cantilever is then reduced to 6.0×10^{-26} N, which is supposed to be limited by the FEA calculation precision.

Magnetic shielding requires the NbTi film to be superconductive, thus requiring the superconducting critical current to be larger than 1.0×10^9 A/m^2 for a coating thickness of 1.5 μm, according to the FEA simulation. The requirement for the critical current is usually achievable for a NbTi film. If a thicker superconducting film is used, the requirement for the critical current will be less stringent. On the other hand, we also require that the magnetic field is lower than the lower critical field of the NbTi film at the interface between the magnetic loop and the superconducting thin film. This requires that the permanent magnet film should not be thicker than the soft magnet film to make the magnetic field lower than the lower critical field, which is around 73 mT [46].

B. Casimir force

The Casimir force is contributed mainly from the surface layer of the material, where a layer of thickness d contributes about $(1 - e^{-4\pi d/\lambda_p})$ of the Casimir force between two infinitely thick metallic plates [47,48]. Here λ_p is the plasma wavelength of the material. In the proposed experiments, the source structures are coated with either 150-nm-thick gold or 1.5-μm-thick superconducting thin films. For 150-nm-thick gold film, $e^{-4\pi d/\lambda_p} \sim 10^{-6}$, which means that the Casimir force difference due to different materials under the coating should be smaller than 10^{-21} N. Thus, here we focus on the variation of the Casimir force due to surface corrugation. The Casimir force is then estimated by proximity force approximation [49,50]. The Casimir energy between two surfaces at a short distance can be approximated as

$$U^{Ca} = \iint_D E_{pp}(z)\mathrm{d}x\mathrm{d}y, \tag{9}$$

where D stands for the projection of the tip to the x-y plane, with x and y being the integral variables, $E_{pp}(z)$ stands for the Casimir energy per unit area of two electrically neutral, infinitely large, parallel conducting planes at a distance of z. Here we use $E_{pp}(z) = -\pi^2 \hbar c / 720 z^3$, the Casimir energy density of a perfect conductor, as a conservative estimation.

To estimate the component of the same period as the source structure, the source surface is modeled as $z = z_0 + z_1 \sin(2\pi y/\Lambda)$, where z_0 is the mean level of the surface, z_1 is the surface wave amplitude, and Λ is the source structure period. In previous experiments, the

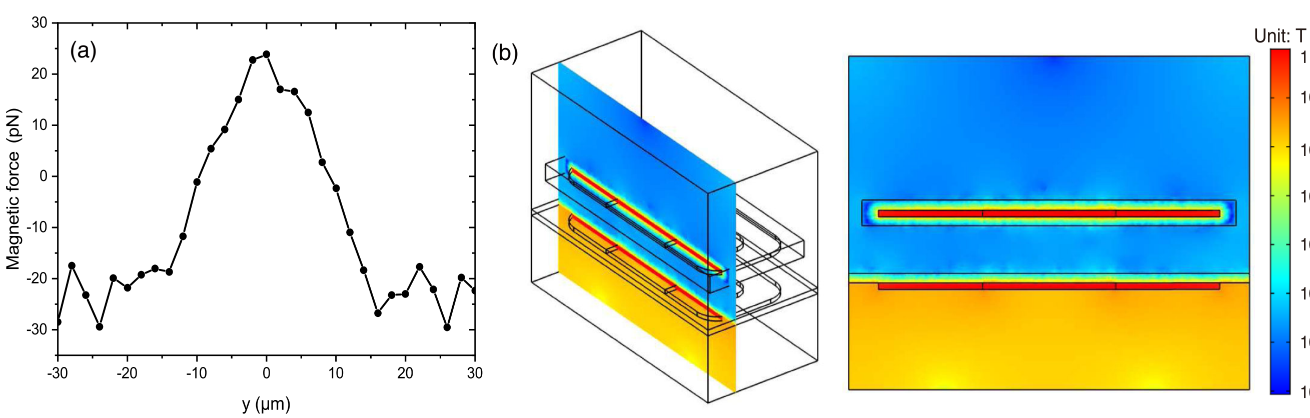

FIG. 9. (a) FEA simulation of the magnetic force between two CLMSs as a function of the lateral relative position. (b) Magnetic flux density distribution around the superconducting shielded CLMS on the cantilever and the source.

periodic variation in surface height could be reduced to 3 nm using a SOI-wafer-based fabrication process [45]. With $z_1 = 3$ nm, we estimate the variation amplitude of the Casimir force between the tip and source structure to be 6.9×10^{-20} N at a tip-surface distance of 2 μm. The variation of the Casimir force acting on the source structure is 2.1×10^{-19} N by the surface of the CLMS, and 3.5×10^{-20} N by the remaining area of the cantilever. All of the above are much smaller than the minimum detectable force.

C. Electrostatic force

The electrostatic force is another important spurious force that exists in many precision measurement experiments [51–54]. As with the Casimir force, we are more concerned with the spatially varying force component of the same period as the source structure. These components may arise from the surface corrugation associated with the periodic structure, or from the surface patch potential. Since the structures are complicated, we employ the FEA here to calculate the electrostatic force.

We use the same surface model and tip-surface distance as in the Casimir force calculation. The average residual potential difference can be compensated to around 2 mV by applying a voltage between the tip and the source. The variation amplitude of the electrostatic force is then estimated to be 6.5×10^{-20} N between the tip and the source, 5.3×10^{-20} N between the CLMS on the cantilever and the source, and 7.0×10^{-19} N between the remaining area of the cantilever and the source. We see that the variation contributed from the surface corrugation is much smaller than the minimum detectable force.

Patch surface charges are generally randomly distributed over the surface, but their distribution may have the component of the same period as the source structure. To estimate this contribution, we assume that the source surface potential is described as $V(x, y) = V_0 + V_1 \sin(2\pi y/\Lambda)$, which refers to the tip. Here V_0 is the average potential difference after compensation and V_1 is the potential fluctuation on the source surface. Based on the calculation, in order to make the patch electrostatic force less than the minimum detectable force, we need to make a flat clean surface with a potential fluctuation of less than 1 mV, where the variation amplitude of the electrostatic force is 1.4×10^{-17} N between the tip and the source, 4.0×10^{-17} N between the CLMS on the cantilever and the source, and 1.9×10^{-17} N between the remaining area of the cantilever and the source. The actual electrostatic force can be evaluated using data obtained by atomic force microscopy and Kelvin probe force microscopy (KPFM). The commercially available KPFM can measure the surface potential with a precision of ∼1 mV and a lateral resolution of ∼10 nm [55]. Using a gold-coated microsphere as the probe could improve the potential measurement precision, but still with enough lateral resolution at around a micrometer, which is plausible for the patch electrostatic force evaluation.

V. CONCLUSION

In conclusion, we have described the experiments to search for the exotic V_2 and V_3 interactions by measuring the force between a CLMS and different spin-polarized source structures. Several measures have been taken to suppress the spurious magnetic force, including the closed-loop magnetic structure design, superconducting magnetic shielding, and periodic spin source structures. The magnetic force, as well as the Casimir force and electrostatic force, is expected to be lower than the minimum detectable force, thanks to those special designs. With the force sensitivity of the cantilever operating at low temperatures, the proposed experiments are expected to explore parameter spaces that are about seven orders of magnitude smaller than the current stringent constraints on V_2, and one order of magnitude smaller for V_3. Furthermore, since the V_2 experiment is insensitive to the detection of V_3 interaction, we can unequivocally determine the strength of V_2 and then perform a joint analysis to obtain the magnitude of the V_3 interaction, assuming that they can both exist.

ACKNOWLEDGMENTS

We are indebted to Yiqiu Ma for the helpful discussions and suggestions. This work was supported by the National Key R&D Program of China (Grant No. 2022YFC2204100) and the National Natural Science Foundation of China (Grants No. 11875137 and No. 91736312).

APPENDIX: SIMULATION OF SUPERCONDUCTING SHIELDING EFFECT

The magnetic shielding effect is simulated with COMSOL Multiphysics. In the superconducting region, we implement the equation combining Ampere's and Faraday's laws for the magnetic field $\boldsymbol{H}$ [56], which is given by

$$\nabla \times (\rho \nabla \times \boldsymbol{H}) = -\mu_0 \frac{\partial \boldsymbol{H}}{\partial t}, \tag{A1}$$

where ρ is the resistivity. The superconductor is modeled with a nonlinear resistivity [57]

$$\rho = \frac{E_c}{J_c}\left(\frac{|\boldsymbol{J}|}{J_c}\right)^{n-1}, \tag{A2}$$

where $\boldsymbol{J}$ is the current density, J_c is the critical current density, $n = 40$ is the power law exponent, and $E_c = 1$ μV/cm is the critical electrical field. We take 1.0×10^{10} A/m^2 as the J_c value, which is usually achievable for NbTi films [58].

For the nonsuperconducting region, we use the magnetic scalar potential ϕ defined as $\boldsymbol{H} = -\boldsymbol{\nabla}\phi$. The equation to be solved is $\boldsymbol{\nabla} \cdot \boldsymbol{\nabla}\phi = 0$. The permanent magnet is modeled with a magnetization of 800 kA/m, and the soft magnet is modeled with a relative magnetic permeability of 8000. A minimum thickness of 1.5 μm is determined for the superconducting film to shield the magnetic force. To simulate the periodic structures, we apply periodic boundary conditions in the x and y directions. The magnetic field can be solved by setting appropriate boundary conditions for the magnetic field and magnetic flux density. The magnetic force acting on the cantilever is calculated by integrating the Maxwell stress tensor over the outer surface of the superconducting film on the cantilever.

[1] E. G. Adelberger, J. Gundlach, B. Heckel, S. Hoedl, and S. Schlamminger, Torsion balance experiments: A low-energy frontier of particle physics, Prog. Part. Nucl. Phys. **62**, 102 (2009).

[2] M. S. Safronova, D. Budker, D. DeMille, Derek F. Jackson Kimball, A. Derevianko, and C. W. Clark, Search for new physics with atoms and molecules, Rev. Mod. Phys. **90**, 025008 (2018).

[3] F. Ficek and D. Budker, Constraining exotic interactions, Ann. Phys. (Berlin) **531**, 1800273 (2019).

[4] J. E. Moody and F. Wilczek, New macroscopic forces?, Phys. Rev. D **30**, 130 (1984).

[5] P. Fayet, The fifth interaction in grand-unified theories: A new force acting mostly on neutrons and particle spins, Phys. Lett. B **172**, 363 (1986).

[6] P. Fayet, New interactions and the standard models, Classical Quantum Gravity **13**, A19 (1996).

[7] B. A. Dobrescu, Massless Gauge Bosons other than the Photon, Phys. Rev. Lett. **94**, 151802 (2005).

[8] B. A. Dobrescu and I. Mocioiu, Spin-dependent macroscopic forces from new particle exchange, J. High Energy Phys. 11 (2006) 005.

[9] P. Fadeev, Y. V. Stadnik, F. Ficek, M. G. Kozlov, V. V. Flambaum, and D. Budker, Revisiting spin-dependent forces mediated by new bosons: Potentials in the coordinate-space representation for macroscopic- and atomic-scale experiments, Phys. Rev. A **99**, 022113 (2019).

[10] R. D. Peccei and H. R. Quinn, *CP* Conservation in the Presence of Pseudoparticles, Phys. Rev. Lett. **38**, 1440 (1977).

[11] S. Weinberg, A New Light Boson?, Phys. Rev. Lett. **40**, 223 (1978).

[12] F. Wilczek, Problem of Strong *P* and *T* Invariance in the Presence of Instantons, Phys. Rev. Lett. **40**, 279 (1978).

[13] J. E. Kim and G. Carosi, Axions and the strong *CP* problem, Rev. Mod. Phys. **82**, 557 (2010).

[14] G. Bertone, D. Hooper, and J. Silk, Particle dark matter: Evidence, candidates and constraints, Phys. Rep. **405**, 279 (2005).

[15] N. Arkani-Hamed, D. P. Finkbeiner, T. R. Slatyer, and N. Weiner, A theory of dark matter, Phys. Rev. D **79**, 015014 (2009).

[16] E. J. Copeland, M. Sami, and S. Tsujikawa, Dynamics of dark energy, Int. J. Mod. Phys. D **15**, 1753 (2006).

[17] P. J. E. Peebles and B. Ratra, The cosmological constant and dark energy, Rev. Mod. Phys. **75**, 559 (2003).

[18] M. Kamionkowski, J. Pradler, and D. G. E. Walker, Dark Energy from the String Axiverse, Phys. Rev. Lett. **113**, 251302 (2014).

[19] N. Arkani-Hamed, S. Dimopoulos, and G. Dvali, The hierarchy problem and new dimensions at a millimeter, Phys. Lett. B **429**, 263 (1998).

[20] P. W. Graham, D. E. Kaplan, and S. Rajendran, Cosmological Relaxation of the Electroweak Scale, Phys. Rev. Lett. **115**, 221801 (2015).

[21] L. Di Luzio, M. Giannotti, E. Nardi, and L. Visinelli, The landscape of QCD axion models, Phys. Rep. **870**, 1 (2020).

[22] P. W. Graham, I. G. Irastorza, S. K. Lamoreaux, A. Lindner, and K. A. van Bibber, Experimental searches for the axion and axion-like particles, Annu. Rev. Nucl. Part. Sci. **65**, 485 (2015).

[23] P. Sikivie, Invisible axion search methods, Rev. Mod. Phys. **93**, 015004 (2021).

[24] D. J. Wineland, J. J. Bollinger, D. J. Heinzen, W. M. Itano, and M. G. Raizen, Search for Anomalous Spin-Dependent Forces Using Stored-Ion Spectroscopy, Phys. Rev. Lett. **67**, 1735 (1991).

[25] A. G. Glenday, C. E. Cramer, D. F. Phillips, and R. L. Walsworth, Limits on Anomalous Spin-Spin Couplings between Neutrons, Phys. Rev. Lett. **101**, 261801 (2008).

[26] G. Vasilakis, J. M. Brown, T. W. Kornack, and M. V. Romalis, Limits on New Long Range Nuclear Spin-Dependent Forces Set with a K-^{3}He Comagnetometer, Phys. Rev. Lett. **103**, 261801 (2009).

[27] M. P. Ledbetter, M. V. Romalis, and D. F. Jackson Kimball, Constraints on Short-Range Spin-Dependent Interactions from Scalar Spin-Spin Coupling in Deuterated Molecular Hydrogen, Phys. Rev. Lett. **110**, 040402 (2013).

[28] L. Hunter, J. Gordon, S. Peck, D. Ang, and J.-F. Lin, Using the Earth as a polarized electron source to search for long-range spin-spin interactions, Science **339**, 928 (2013).

[29] S. Kotler, R. Ozeri, and Derek F. Jackson Kimball, Constraints on Exotic Dipole-Dipole Couplings between Electrons at the Micrometer Scale, Phys. Rev. Lett. **115**, 081801 (2015).

[30] P. Luo, J. Ding, J. Wang, and X. Ren, Constraints on spin-dependent exotic interactions between electrons at the nanometer scale, Phys. Rev. D **96**, 055028 (2017).

[31] W. Ji, C. B. Fu, and H. Gao, Searching for new spin-dependent interactions with $SmCo_5$ spin sources and a spin-exchange-relaxation-free comagnetometer, Phys. Rev. D **95**, 075014 (2017).

[32] F. Ficek, Derek F. Jackson Kimball, M. G. Kozlov, N. Leefer, S. Pustelny, and D. Budker, Constraints on exotic spin-dependent interactions between electrons from helium fine-structure spectroscopy, Phys. Rev. A **95**, 032505 (2017).

[33] F. Ficek, P. Fadeev, V. V. Flambaum, D. F. Jackson Kimball, M. G. Kozlov, Y. V. Stadnik, and D. Budker, Constraints on Exotic Spin-Dependent Interactions between Matter and Antimatter from Antiprotonic Helium Spectroscopy, Phys. Rev. Lett. **120**, 183002 (2018).

[34] X. Rong, M. Jiao, J. Geng, B. Zhang, T. Xie, F. Shi, C.-K. Duan, Y.-F. Cai, and J. Du, Constraints on a Spin-Dependent Exotic Interaction between Electrons with Single Electron Spin Quantum Sensors, Phys. Rev. Lett. **121**, 080402 (2018).

[35] A. Almasi, J. Lee, H. Winarto, M. Smiciklas, and M. V. Romalis, New Limits on Anomalous Spin-Spin Interactions, Phys. Rev. Lett. **125**, 201802 (2020).

[36] Y. Wang, H. Su, M. Jiang, Y. Huang, Y. Qin, C. Guo, Z. Wang, D. Hu, W. Ji, P. Fadeev, X. Peng, and D. Budker, Limits on Axions and Axionlike Particles within the Axion Window Using a Spin-Based Amplifier, Phys. Rev. Lett. **129**, 051801 (2022).

[37] R. C. Ritter, C. E. Goldblum, W.-T. Ni, G. T. Gillies, and C. C. Speake, Experimental test of equivalence principle with polarized masses, Phys. Rev. D **42**, 977 (1990).

[38] B. R. Heckel, W. A. Terrano, and E. G. Adelberger, Limits on Exotic Long-Range Spin-Spin Interactions of Electrons, Phys. Rev. Lett. **111**, 151802 (2013).

[39] W. A. Terrano, E. G. Adelberger, J. G. Lee, and B. R. Heckel, Short-Range, Spin-Dependent Interactions of Electrons: A Probe for Exotic Pseudo-Goldstone Bosons, Phys. Rev. Lett. **115**, 201801 (2015).

[40] T. M. Leslie, E. Weisman, R. Khatiwada, and J. C. Long, Prospects for electron spin-dependent short-range force experiments with rare earth iron garnet test masses, Phys. Rev. D **89**, 114022 (2014).

[41] T. C. P. Chui and W.-T. Ni, Experimental Search for an Anomalous Spin-Spin Interaction between Electrons, Phys. Rev. Lett. **71**, 3247 (1993).

[42] J. Ding, J. Wang, X. Zhou, Y. Liu, K. Sun, A. O. Adeyeye, H. Fu, X. Ren, S. Li, P. Luo, Z. Lan, S. Yang, and J. Luo, Constraints on the Velocity and Spin Dependent Exotic Interaction at the Micrometer Range, Phys. Rev. Lett. **124**, 161801 (2020).

[43] B. Glaubitz, S. Buschhorn, F. Brüssing, R. Abrudan, and H. Zabel, Development of magnetic moments in $Fe_{1-x}Ni_x$-alloys, J. Phys. Condens. Matter **23**, 254210 (2011).

[44] J. Wang, S. Guan, K. Chen, W. Wu, Z. Tian, P. Luo, A. Jin, S. Yang, C. Shao, and J. Luo, Test of non-Newtonian gravitational forces at micrometer range with two-dimensional force mapping, Phys. Rev. D **94**, 122005 (2016).

[45] X. Ren, J. Wang, R. Luo, L. Yin, J. Ding, G. Zeng, and P. Luo, Search for an exotic parity-odd spin- and velocity-dependent interaction using a magnetic force microscope, Phys. Rev. D **104**, 032008 (2021).

[46] S. L. Naour, L. Oberli, R. Wolf, R. Puzniak, A. Szewczyk, A. Wisniewski, H. Fikis, M. Foitl, and H. Kirchmayr, Magnetization measurements on LHC superconducting strands, IEEE Trans. Appl. Supercond. **9**, 1763 (1998).

[47] R. S. Decca, D. López, H. B. Chan, E. Fischbach, D. E. Krause, and C. R. Jamell, Constraining New Forces in the Casimir Regime Using the Isoelectronic Technique, Phys. Rev. Lett. **94**, 240401 (2005).

[48] R. Matloob and H. Falinejad, Casimir force between two dielectric slabs, Phys. Rev. A **64**, 042102 (2001).

[49] M. Bordag, G. L. Klimchitskaya, U. Mohideen, and V. M. Mostepanenko, *Advances in the Casimir Effect* (Oxford University Press, New York, 2009).

[50] J. Blocki, J. Randrup, W. Swiatecki, and C. Tsang, Proximity forces, Ann. Phys. (N.Y.) **105**, 427 (1977).

[51] N. A. Robertson, J. R. Blackwood, S. Buchman, R. L. Byer, J. Camp, D. Gill, J. Hanson, S. Williams, and P. Zhou, Kelvin probe measurements: Investigations of the patch effect with applications to ST-7 and LISA, Classical Quantum Gravity **23**, 2665 (2006).

[52] W. J. Kim, A. O. Sushkov, D. A. R. Dalvit, and S. K. Lamoreaux, Surface contact potential patches and Casimir force measurements, Phys. Rev. A **81**, 022505 (2010).

[53] C. C. Speake, Forces and force gradients due to patch fields and contact-potential differences, Classical Quantum Gravity **13**, A291 (1996).

[54] H. Yin, Y.-Z. Bai, M. Hu, L. Liu, J. Luo, D.-Y. Tan, H.-C. Yeh, and Z.-B. Zhou, Measurements of temporal and spatial variation of surface potential using a torsion pendulum and a scanning conducting probe, Phys. Rev. D **90**, 122001 (2014).

[55] Y. Masatoshi, Improvement of Kelvin probe force microscope (KFM) system, Jpn. J. Appl. Phys. **34**, 3403 (1995).

[56] A. Arsenault, F. Sirois, and F. Grilli, Implementation of the H-ϕ formulation in COMSOL Multiphysics for simulating the magnetization of bulk superconductors and comparison with the H-formulation, IEEE Trans. Appl. Supercond. **31**, 1 (2021).

[57] J. Rhyner, Magnetic properties and AC-losses of superconductors with power law current—Voltage characteristics, Physica (Amsterdam) **212C**, 292 (1993).

[58] M. Takeda and K. Nishigaki, Influence of thickness on parallel and perpendicular field dependences of J_c of NbTi films, Physica (Amsterdam) **357C–360C**, 1373 (2001).